

Article

Innovative Structural Optimization and Dynamic Performance Enhancement of High-Precision Five-Axis Machine Tools

Ratnakar Behera, Tzu-Chi Chan *  and Jyun-Sian Yang

Department of Mechanical and Computer-Aided Engineering, National Formosa University,
Yunlin County 632, Taiwan; d1281109@nfu.edu.tw (R.B.)

* Correspondence: tcchan@nfu.edu.tw; Tel.: +886-928985183; Fax: +886-5-6315310

Abstract: To satisfy the requirements of five-axis processing quality, this article improves and optimizes the machine tool structure design to produce improved dynamic characteristics. This study focuses on the investigation of five-axis machine tools' static and dynamic stiffness as well as structural integrity. We also include performance optimization and experimental verification. We use the finite element approach as a structural analysis tool to evaluate and compare the individual parts of the machine created in this study, primarily the saddle, slide table, column, spindle head, and worktable. We discuss the precision of the machine tool model and relative space distortion at each location. To meet the requirements of the actual machine, we optimize the structure of the five-axis machine tool based on the parameters and boundary conditions of each component. The machine's weight was 15% less than in the original design model, the material it was subjected to was not strained, and the area of the structure where the force was considerably deformed was strengthened. We evaluate the AM machine's impact resistance to compare the vibrational deformation observed in real time with the analytical findings. During modal analysis, all the order of frequencies were determined to be 97.5, 110.4, 115.6, and 129.6 Hz. The modal test yielded the following orders of frequencies: 104, 118, 125, and 133 Hz. Based on the analytical results, the top three order error percentages are +6.6%, +6.8%, +8.1%, and +2.6%. In ME'scope, the findings of the modal test were compared with the modal assurance criteria (MAC) analysis. According to the static stiffness analysis's findings, the main shaft and screw have quite substantial major deformations, with a maximum deformation of 33.2 μm . Force flow explore provides the relative deformation amount of 26.98 μm from the rotating base (C) to the tool base, when a force of 1000 N is applied in the X-axis direction, which is more than other relative deformation amounts. We also performed cutting transient analysis, cutting spectrum analysis, steady-state thermal analysis, and analysis of different locations of the machine tool. All of these improvements may effectively increase the stiffness of the machine structure as well improve the machine's dynamic characteristics and increases its machining accuracy. The topology optimization method checks how the saddle affects the machine's stability and accuracy. This research will boost smart manufacturing in the machine tool sector, leading to notable advantages and technical innovations.

Keywords: multi-axis machining tool; finite element method; vibration mode analysis; modal test; harmonic analysis; optimizations; steady-state thermal analysis



Citation: Behera, R.; Chan, T.-C.; Yang, J.-S. Innovative Structural Optimization and Dynamic Performance Enhancement of High-Precision Five-Axis Machine Tools. *J. Manuf. Mater. Process.* **2024**, *8*, 181. <https://doi.org/10.3390/jmmp8040181>

Academic Editor: Steven Y. Liang

Received: 11 July 2024

Revised: 8 August 2024

Accepted: 12 August 2024

Published: 19 August 2024



Copyright: © 2024 by the authors. Licensee MDPI, Basel, Switzerland. This article is an open access article distributed under the terms and conditions of the Creative Commons Attribution (CC BY) license (<https://creativecommons.org/licenses/by/4.0/>).

1. Introduction

In today's global marketplace, machine tools are vital for fostering innovation and competitiveness. They enable producers to quickly iterate through new designs, streamline production processes, and adapt to the ever-changing needs of the market. Thus, the goal of this study is to bring computer-aided engineering analysis technology and utilize a five-axis machine tool, a novel innovation tool.

As far as we are aware, Yutian et al. [1] presented the design and development of a five-axis machine tool for aero-engine casing manufacturing. Machine tool development

has always aimed for increased efficiency and precision, and some successful studies have been conducted in this area by academics. For example, there have been studies on geometric error modeling, identification and compensation [2–4], thermal error prediction and compensation [5,6], and spindle accuracy measuring [7,8]. Among all studies, the design and development of a machine tool [9,10] can be considered as the essential issue. Chan et al. [11] investigated the effect of spatial moving structure and topology optimization of CNC turning machine tools. Shen Lei et al. [12] investigated the machine tool's structural dynamic design, optimization, and experimental validation. Wu et al. [13] studied a five-DOF hybrid machining tool featuring forced vibrations in a two-DOF parallel manipulator and developed a corresponding mechatronics model. Chan et al. [14] investigated the three-axis machining center's kinematic structure performance and machining features. Gegg et al. [15] examined the application of axial ultrasonic vibrations during milling operations, which enhanced the process by decreasing cutting forces and increasing surface smoothness. Zhou et al. [16] explored and introduced an innovative method for modeling and predicting ball screw thermal deformation, moving beyond reliance solely on CNC real-time data and temperature sensor information. A review of five-axis CNC milling machine tool operations has also been carried out [17]. An experiential modal analysis (EMA) method based on a frequency response function (FRF) was proposed by Chan et al. [18] for system vibration monitoring. Modal simulation and harmonic response analysis are conducted to predict an additive manufacturing system's dynamic characteristics and deformation errors with moving elements at different spatial positions [19]. The spatial accuracy and compensation of the Coordinate Measuring Machine are evaluated using the finite element method. This analysis encompasses static deformation, modal analysis, spectral analysis, and transient assessments [20]. Vibration mode analysis was implemented to connect experimental methods with finite element simulations to enhance the machine's performance and look into the dynamic aspects of the design process [21]. Lima et al. (2024) [22] investigated a centrifugal compressor impeller's modal analysis and structural optimization. Ramesh et al. [23] conducted evaluations of a crankshaft's harmonic response and mode. Several stages of the manufacturing process need and benefit from knowledge of the cutting force. Tool wear is being tracked increasingly by the measurement of cutting force [24,25]. Ulrika et al. [26] presented an innovative approach for forecasting the fatigue lifespan of vehicle components by combining limited in-service vibration data with finite element modeling. Chan et al. [27] studied the construction of a five-axis, high-speed moving column machine tool and carried out its structural optimization and analysis. Based on the finite element analysis, a design optimization approach for the reactive material structure is established. Topology optimization is presented to decide the structure's form based on the model [28]. The ideal form that can be built and the manufacturing restrictions are taken into consideration while proposing the design variables and optimization constraints. Lacalle et al. [29] focus on providing error-free algorithms that employ the best cutting techniques for surface quality and efficiency, leading to a more dependable production process. The CAM approach has to incorporate additional control and optimization processes to reduce the potential for hazards such as tool breakage and collisions that may harm ceramic bearings in the spindles. Significant advances in industrial development are being driven by the deployment of five-axis machines through the use of various approaches and techniques [30–33].

The manufacturing sector always looks for new and creative ways to improve machining processes' efficiency, accuracy, and productivity. Under these circumstances, applying sophisticated modeling and simulation methods has become a viable path toward optimizing intricate machining processes. Using five-axis milling methods, which provide greater flexibility and the capacity to produce complex geometries with improved surface quality, is a tough challenge in modern machining. Understanding the dynamic interactions between cutting tools, workpieces, and machine tool components requires the modeling and simulation of these processes. Researchers and practitioners can improve machining parameters, save production costs, and shorten lead times by properly predicting tool

trajectories, cutting forces, chip generation, and surface finishes [34]. Palmai et al. [35] studied the importance of accurately determining cutting forces in milling, noting the impact of transient processes on the entire cutting cycle and developing a validated mathematical model for the decay process during intermittent cutting. Additionally, virtual experimentation made possible by modeling and simulation enables the investigation of different machining tactics and the evaluation of their effects on component quality and process stability.

To shed light on the difficulties, chances, and potential paths forward in this important field, in this work, we explore the most recent approaches to and developments in simulation, including modal analysis, cutting transient analysis, cutting spectrum analysis, optimization, and static analysis of vertical five-axis milling machine tools.

The remainder of this work is provided in the order listed below. In summary, the Materials and Methods are explained in Section 2. This part properly explains finite element modeling, boundary limitations, and constraints, as well as the flow chart of research methodologies. We first create the optimized finite element model and then proceed with the modal analysis, harmonic response, and static stiffness analysis. Experimental modal testing is covered in Section 3. An impact hammer is used in this step for modal testing. A comparison of the outcomes of modal analysis and modal testing is shown in Section 4. Recommendations for further research are provided at the end of Section 5.

2. Materials and Methods

2.1. Material

The materials for the vertical milling machine in this investigation were tungsten carbide, gray cast iron, and S40C medium carbon steel. Table 1 lists the material qualities of these items.

Table 1. Material properties.

Gray Cast Iron	
Density (kg/m ³)	7200
Young’s modulus (Pa)	1.24 × 10 ¹¹
Poisson’s ratio	0.3
Hardness, Rockwell C	20
S40C medium carbon steel	
Density (kg/m ³)	7850
Young’s modulus (Pa)	2 × 10 ¹¹
Poisson’s ratio	0.28
Hardness, Rockwell C	30
Tungsten carbide	
Density (kg/m ³)	15,000
Young’s modulus (Pa)	5.5 × 10 ¹¹
Poisson’s ratio	0.28
Hardness, Rockwell C	70

2.2. Physical Structure of 5-Axis Machine

A 5-axis machine is made up of many essential parts that function as a unit to provide accurate and adaptable machining as shown in Figure 1. For steady functioning, the base and column, which are usually constructed of welded steel or cast iron, offer foundational support and vibration absorption. The cutting tool is rotated at high speeds for precise machining via the spindle, which is composed of materials like high-speed steel, carbide, or ceramics. For complicated geometries, the rotary axes (A and B) and linear axes (X, Y, and Z) made of high-strength steel or aluminum offer the required degrees of freedom. Precise and

seamless motions are guaranteed by ball screws and linear guides composed of hardened steel. By controlling heat and lowering friction, cooling and lubrication systems made of different metals and alloys preserve ideal working conditions. These parts work together to provide the 5-axis machine with the great precision and efficiency needed to complete complex machining operations, which makes it a vital tool in advanced manufacturing.

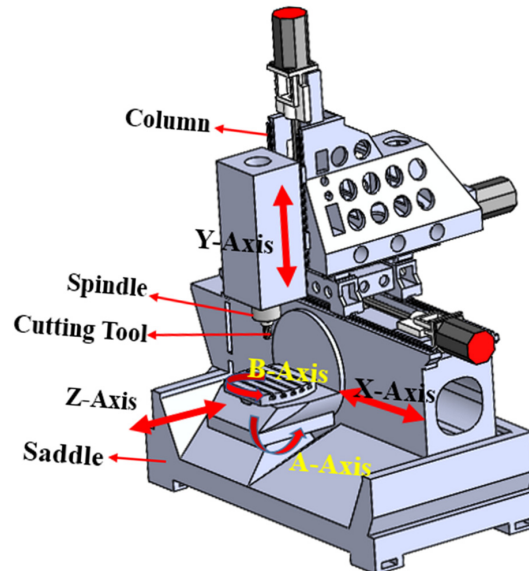


Figure 1. The physical structure of the 5-axis machine used for analysis.

2.3. Research Process

This proposal focuses on conducting structural optimization analysis and constructing a multi-axis machine tool. The machine design is optimized, and performance modifications are analyzed and compared, using the finite element approach. Figure 2 displays the analytical and experimental architecture flowchart.

The material qualities and spring settings of the original 5-axis machine tool are specified after it has undergone complete optimization. A 20 mm mesh size and tetrahedron Solid 187 elements are employed with patch-conforming algorithms and quadratic element order. Every subsequent procedure is completed in order. An impact hammer test is used to compare the outcomes after the FEA code is used for the modal analysis. Static, harmonic, transient, and spectrum analyses are also performed. ME'scope is used to assess the modal assurance criteria (MAC) to compare the outcomes of modal analysis and modal testing.

A comprehensive finite element model of the 5-axis machine tool is developed using the SolidWorks optimization tool, including detailed representations of all critical components, joints, and interfaces. The initial step involved designing the structural model's appearance. Figure 3 shows the original structure of the machine tool. Then, SolidWorks is used to optimize the structure, identifying the best solution. The model part drawing is then adjusted according to the optimization results, as depicted in Figure 4. In the context of structural and topology optimization, a contour plot of element densities is a crucial tool. The design domain is discretized into finite elements, each assigned a density value from 0 (no material) to 1 (solid material), with intermediate values indicating partial material presence. The contour plot displays the spatial variation of these densities using contour lines or color gradients, making it easy to visualize material distribution. Such a plot helps identify optimal material layout, highlighting areas where material is needed and where it can be removed, thus guiding designers towards the most efficient structure. This optimization led to a 15% weight reduction compared to the original design. Additionally, the material remains unstressed, and significantly deformed areas are reinforced, enhancing the rigidity of the machine structure. Finally, the optimized model design is prepared Figure 5, and to address the problem, a 100 N force was applied to the center of the saddle.

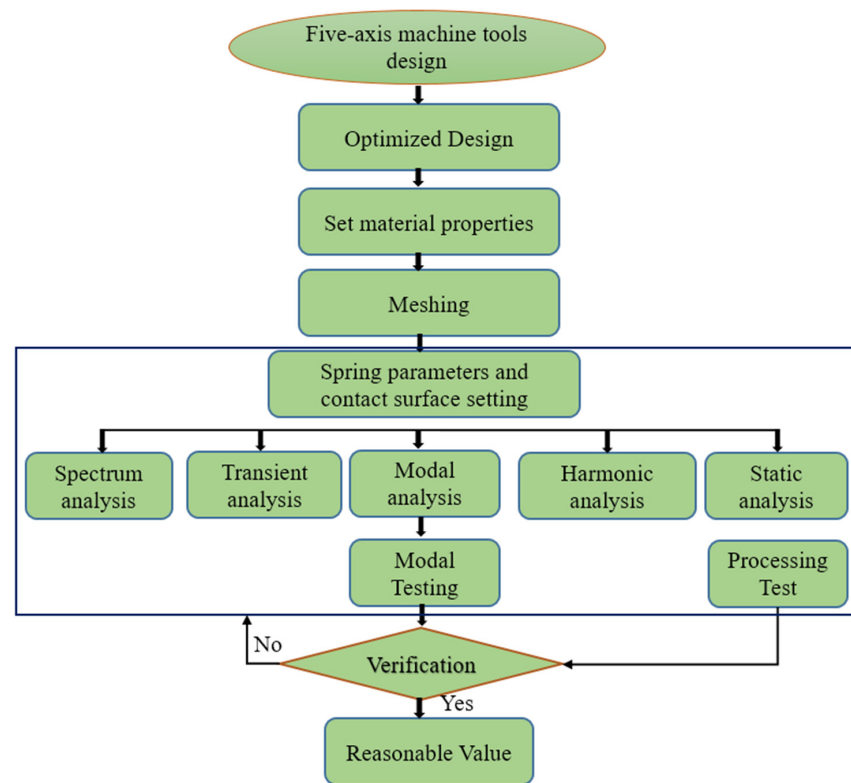


Figure 2. Analysis and experimental architecture flowchart2.4 optimized design.

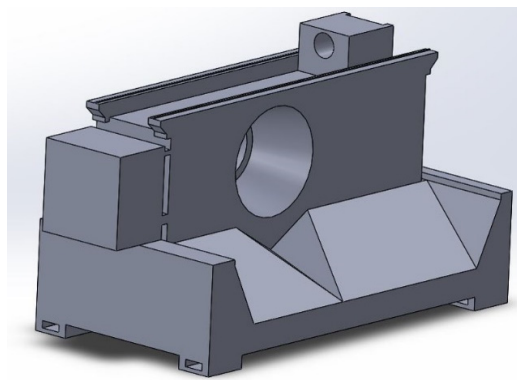


Figure 3. Original base model.

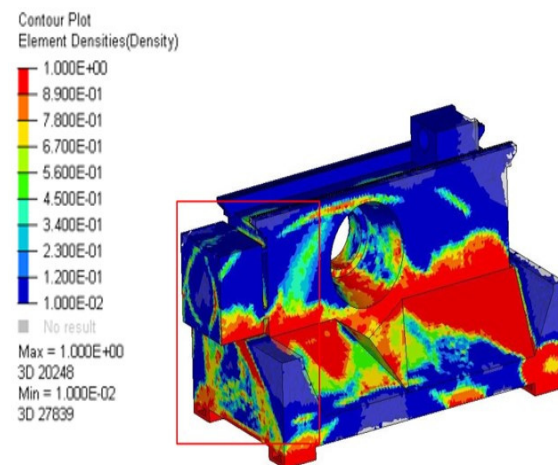


Figure 4. Optimization process of structural force and force streamline distribution.

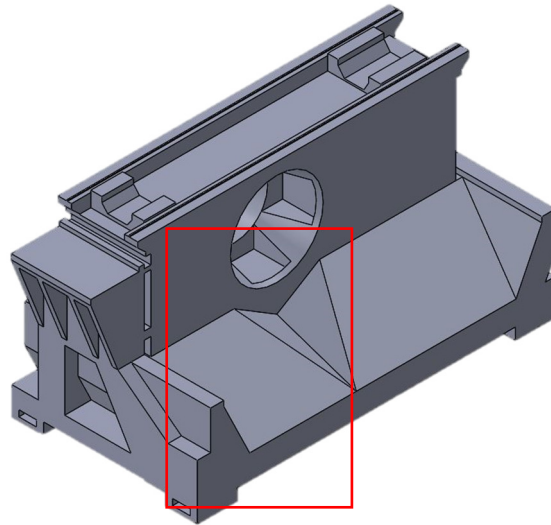


Figure 5. Optimized design base model [27]. The red box shows optimized area comparing to original model.

2.4. Finite Element Analysis

This work constructs a high-order five-axis machine tool, as seen in Figure 6, and examines and optimizes its machine structure. Gray cast iron, S40C medium carbon steel, and tungsten carbide make up the majority of the structural material. A finite element model is created, and boundary interface settings are specified for finite element analysis to investigate the structural features, as seen in Figure 7.

The machine is made up of numerous components, with a spring representing the interaction between the slider and the slide rail. The gravitational acceleration is set at 9.8 m/s^2 , and the spring stiffness is set at $1960 \text{ N}/\mu\text{m}$. The degree is calculated using a non-linear function. The use of tetrahedron Solid 187, patch-conforming algorithms, and quadratic element order significantly enhanced the accuracy of our mesh calculations. There are 713,791 elements and 1,101,810 nodes in the model. Figure 8 shows the FEM model of the vertical 5-axis milling machine.

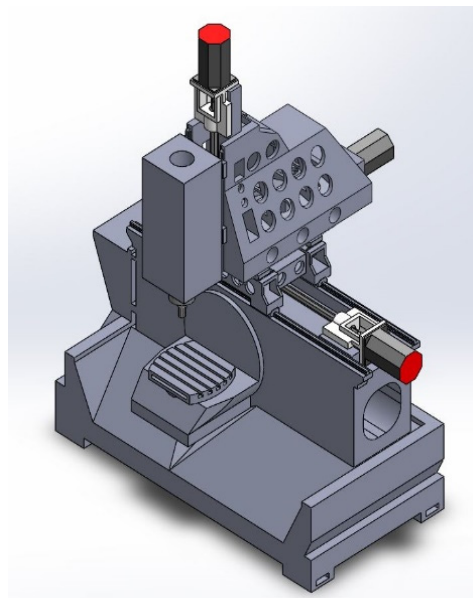


Figure 6. Designed machine model image.

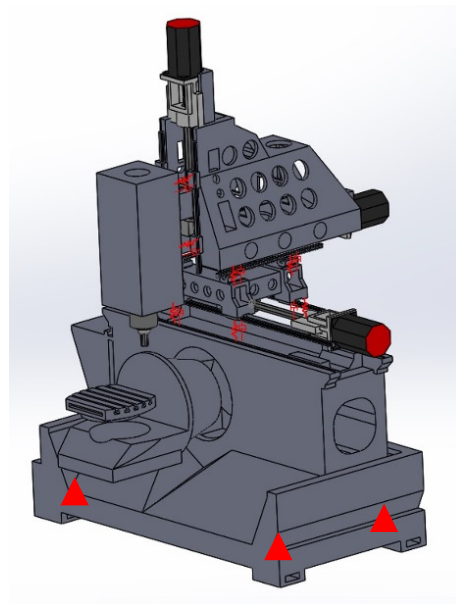


Figure 7. Spring damper boundary conditions.

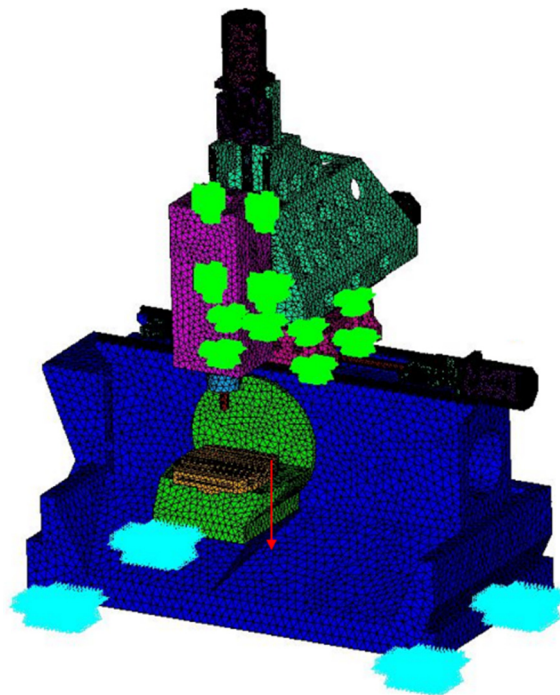


Figure 8. Finite element model of the vertical machine tool.

2.5. Static Stiffness Analysis

The static stiffness of the machine tool was analyzed to determine its ability to resist deformation under static loads. Appropriate boundary conditions were applied to simulate the real-world constraints of the machine tool. The model was solved to obtain the deformation and stress distribution under the applied loads. The stiffness was calculated by relating the applied load to the resulting displacement. Static loads were applied at critical points to evaluate the deformation response. The static stiffness experiment aims to measure the resistance of a machine tool or its components to deformation under a static load, which is crucial for ensuring machining accuracy and stability. In this experiment, the machine tool or component is securely mounted on a test rig, and a precise force application system applies a known static load to specific points on the machine. High-precision displacement sensors or dial gauges measure the resulting deformations, and the static

stiffness is calculated by dividing the applied load by the measured displacement ($N/\mu m$). The stiffness values are compared with theoretical or simulation results, such as those from finite element method (FEM) analysis, to validate the design and optimization processes. Figure 9a shows the simulation results of the static rigidity analysis for the horizontal machine tool. The static stiffness experiment shown in Figure 9b provides quantitative data on the deformation characteristics of the machine tool or component, guiding further design improvements and optimizations to ensure high precision and reliability in machining operations.

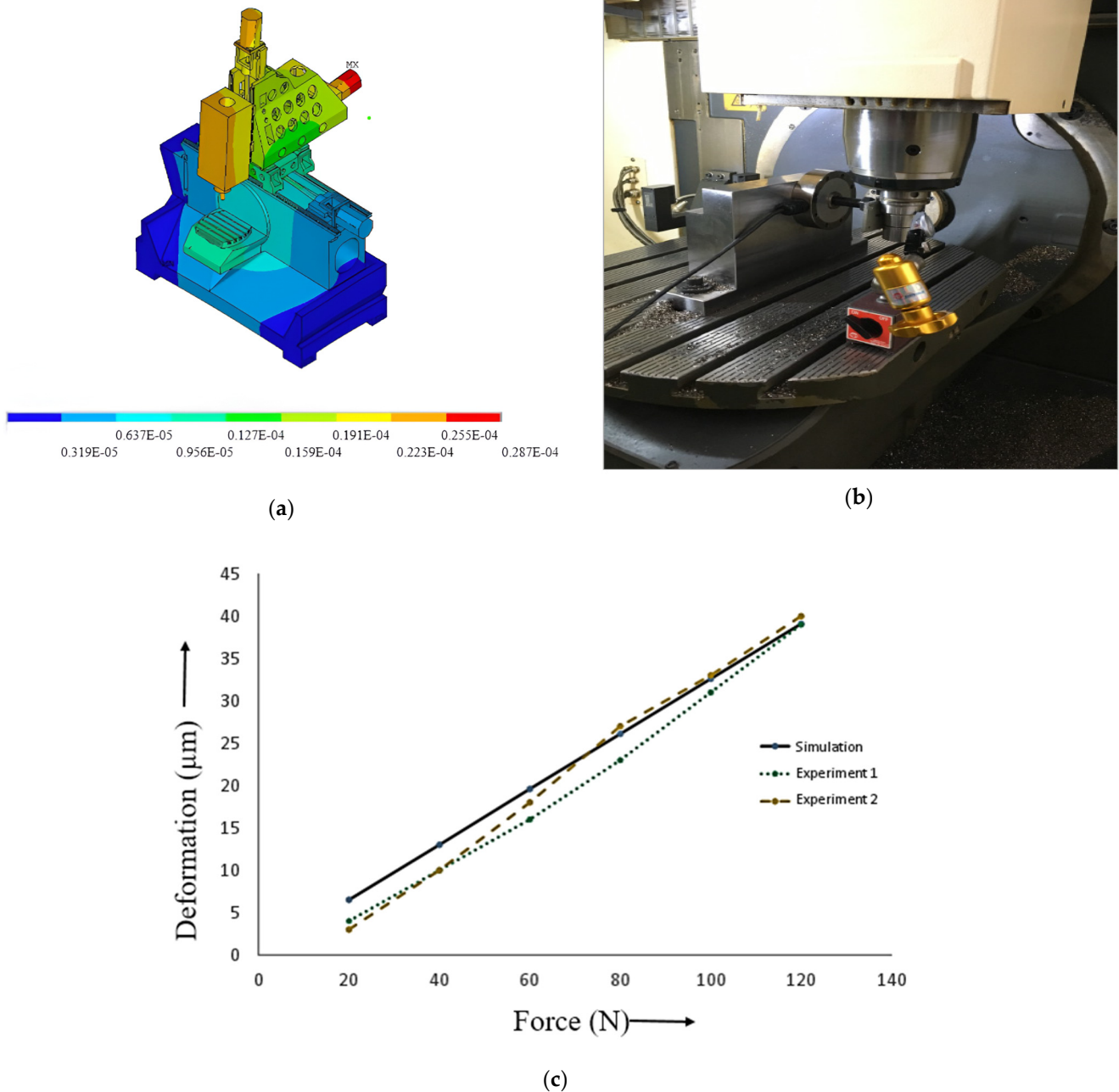


Figure 9. (a) Results of static rigidity analysis of the vertical machine tool through simulation. (b) Static stiffness experiment. (c) Static stiffness simulation and experiment comparison.

During machining, a force of 1000 N is applied in the X direction at the tool tip of the simulation machine. The analysis reveals substantial deformation in both the main shaft and the screw, with the maximum deformation reaching $33.2 \mu m$. The static stiffness analysis yielded a value of $30.0 N/\mu m$, while the experimental measurement was $26.5 N/\mu m$,

resulting in a discrepancy of 11.6% between the test and analysis results. The overall static stiffness of the machine tool meets the design requirements and ensures adequate rigidity for precise machining operations. Figure 9c shows the comparison of static stiffness between the simulation and experiment.

2.6. Modal Analysis

The modal analysis revealed the structure’s dynamic characteristics, identifying key natural frequencies and mode shapes. These insights are vital for design optimization and ensuring operational safety. Based on these findings, we conducted a vibration study. We concluded that avoiding specific frequencies or minimizing their excitation impact to the greatest extent possible will ensure the stability of the machining equipment. The free vibration equation for a damped system can be written as

$$[M]\ddot{x} + [c]\dot{x} + [k]x = 0 \tag{1}$$

The classical eigenvalue issue is undamped modal analysis. The kinematic equation presented by Yu et al. (2017) [36] indicates that the structure’s free vibration is simple harmonic vibration, meaning that the displacement is in line with the sine function.

$$x = x \sin(\omega t) \tag{2}$$

substituting into Equation (1), the following can be obtained:

$$[K] - \omega^2[M][x] = \{0\} \tag{3}$$

Equation (2) is a classic eigenvalue problem; the equation eigenvalue is ω_i^2 , the extraction of a root ω_i is an auto-oscillation circular frequency, the natural vibration frequency is $f = \frac{\omega_i}{2\pi}$ [29]. Vector $\mathbf{1}$ related to ω_i is a mode of vibration related to natural vibration frequency $f = \frac{\omega_i}{2\pi}$. The model was established via SOLIDWORKS 2020. Model data were led into ANSYS18.1 via the interfaces of ANSYS 18.1 and SOLIDWORKS 2020.

The finite element analysis machine is used to analyze the dynamic machine characteristics, and the analysis frequency setting range is 1–1000 Hz. The modal analysis results show frequencies of 97.5, 110.4, 115.6, and 129.6 Hz, and their modal analysis and modal test results are shown in Table 2.

Table 2. Mode shapes and natural frequencies of modal analysis.

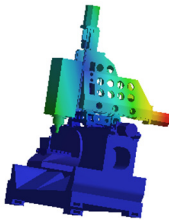
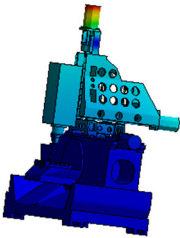
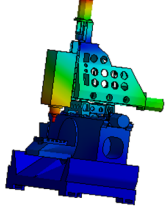
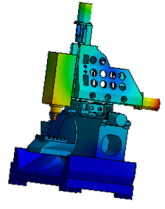
Content	Modal Analysis	Feature
Mode shape 1		Arbor supports machine vibrations
Frequency	97.5 Hz	+6.6%
Mode shape 2		The F=findings of the vibrations from the column.
Frequency	110.4 Hz	+6.8%

Table 2. Cont.

Content	Modal Analysis	Feature
Mode shape 3		The primary movement mechanism for the base section along the Z-axis.
Frequency	115.6 Hz	+8.1%
Mode shape 4		The fourth modal structure's primary distortion mode is the machine bed distortion along the Z-axis.
Frequency	129.6 Hz	+2.6%

2.7. Harmonious Evaluation

Harmonic response analysis is employed to understand how a structure responds to sinusoidal excitation over a particular frequency range. This technique primarily investigates vibration phenomena induced via continuous frequency input and provides valuable insights into the structure's behavior under such oscillatory stimuli [37]. To develop a virtual dynamic model and provide dynamic characteristics for machine tools, Wu et al. (2010) [38] suggested merging modal analysis, harmonic response, and FEA.

The following may be obtained by replacing the dynamic Equation (4) with harmonic force [39]:

$$x(s) = Z^{-1}(s)F(s) = H(s)F(s) \tag{4}$$

where $X(s)$ is the response of the system;

$Z^{-1}(s)$ is the inverse of the impedance matrix;

$F(s)$ is the applied force;

$H(s)$ is the transfer function of the system.

The response function $X(s)$ can be derived from the structure's transfer functions and the input force, even when the excitation (force) changes over time during a dynamic analysis. Beyond machine tool numerical techniques and modal studies, harmonic response analysis can provide a deeper understanding of dynamic characteristics. The machine tool's behavior can be approximated using finite element analysis (FEA). If vibration modes and frequencies fall within a reasonable error range, this may be confirmed using frequency spectrum analysis. The responses of different frequencies are examined by subjecting the spinning cutting tool to an external force. For examination at frequencies ranging from 1 to 200 Hz, a 500 N force was applied to the cutting tool attached to the headstock spindle of the 5-axis machine in this experiment. Figure 10 displays the cutting tool's X-, Y-, and Z-axis frequency responses based on the results.

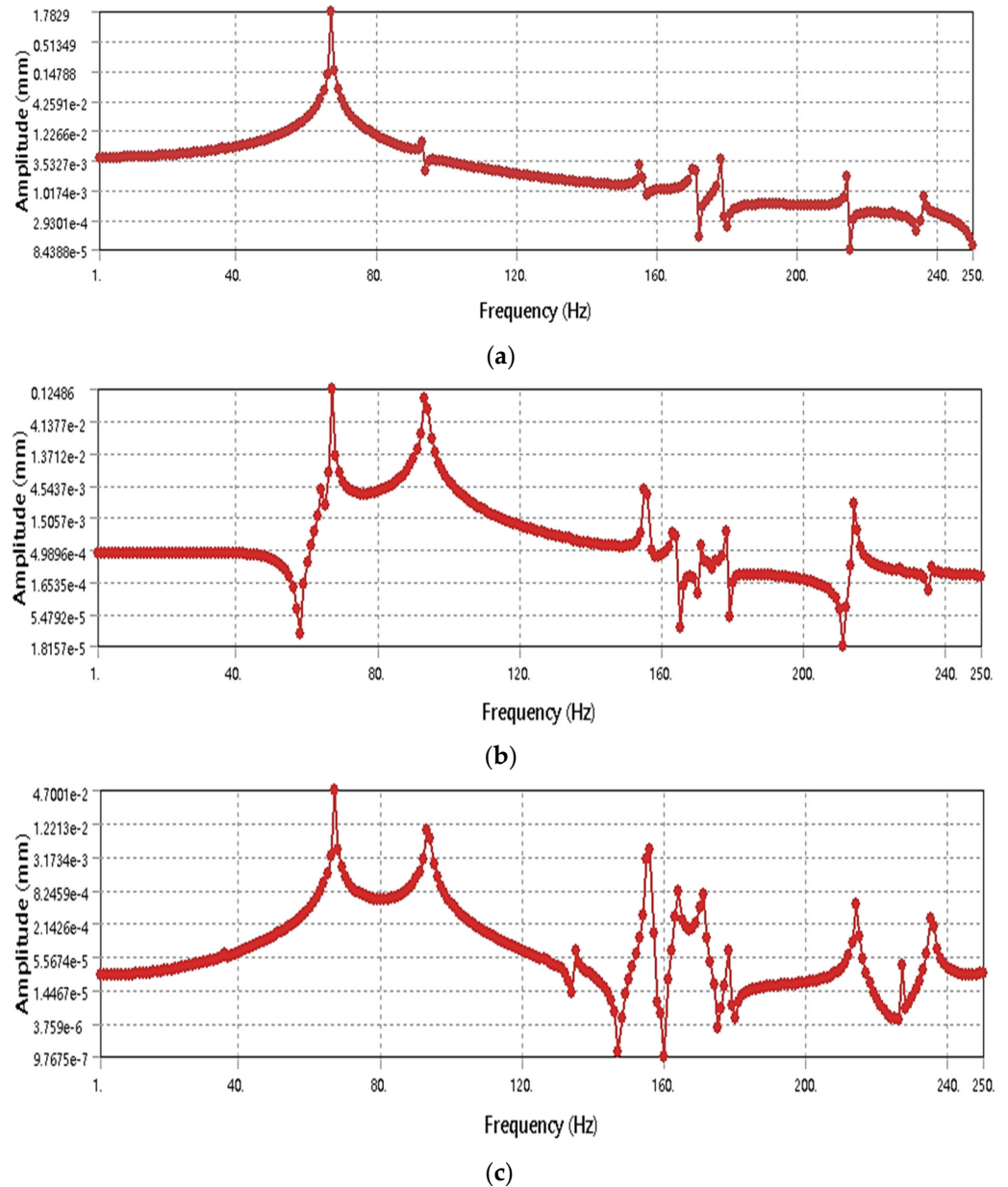


Figure 10. Shows harmonic frequency responses in the X-, Y-, and Z-axis.

2.8. Cutting Transient Analysis

In the transient analysis, an impact force of 100 N was applied to the machine tool. The base of the machine tool was fixed to ensure stability during the test. The specific location of the impact point is illustrated in Figure 11. An extra cutting force was used for 0.05 s to replicate the cutting process. This cutting force induced a vibration response in the machine tool, which was observed and recorded over 2 s. The transient response of the system to the applied forces provided valuable insights into the dynamic behavior of the machining equipment. In Figure 12, the analysis enabled us to determine the amplitude of the tip point response in the X-axis direction. This information is crucial for understanding how the machine tool reacts to sudden forces and for identifying any potential issues related to vibrations that could affect machining accuracy and tool life. By analyzing the response amplitude, we can make informed decisions about necessary design modifications or adjustments to improve the machine’s performance and stability.

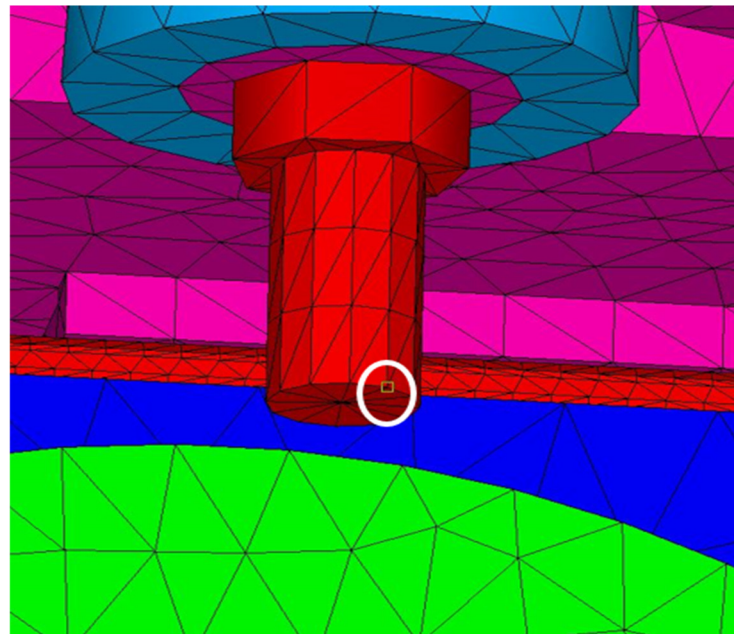


Figure 11. Cutting point of cutting force.

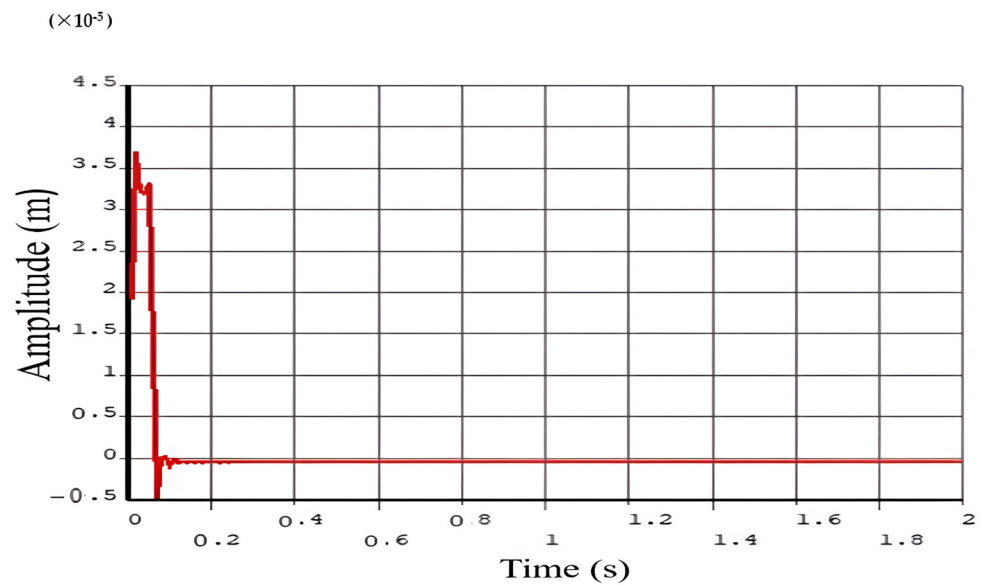


Figure 12. Transient response analysis for the X direction.

2.9. Cutting Spectrum Analysis

Cutting tool precision is greatly dependent on the frequency and amplitude of vibrations of the five-axis machine tool in the Z direction, as seen in Figure 13. Elevated vibration levels may cause tool path deviations, leading to dimensional errors and poor surface quality. By examining the cutting spectrum, resonance circumstances that may exacerbate vibrations and impair machining performance may be found. Critical frequency peaks that need to be reduced in order to maintain process stability are shown in Figure 12. Machining accuracy and surface quality may be significantly increased by minimizing vibration amplitudes via dynamic balancing, dampening improvements, and structural reinforcements.

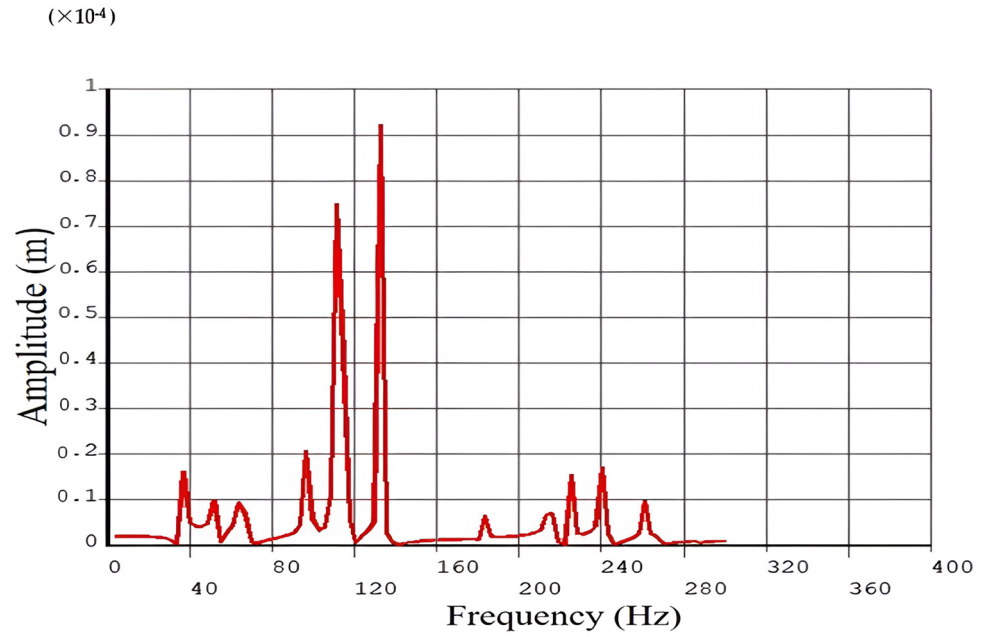


Figure 13. Cutting spectrum analysis in the Z direction.

2.10. Effect of Moving Structure on Dynamic Structure Performance in Different Locations

This study determines the frequency changes at three different locations. Position A is the leftmost end of X, the most forward point of Y, and the uppermost point of Z on the five-axis machine, and mode shapes are 43.9, 60.4, 89.3, and 105.4 Hz, as shown in Figure 14a. Position B is the center of X, the center of Y, and the center of Z, and intermediate mode shapes are 45.6, 70.5, 82.5, and 103.4 Hz, as shown in Figure 14b. Position C is the rightmost end of X, the rear end of Y, and the bottommost point of Z, and mode shapes are 60.2, 95.9, 98.4, and 129.6 Hz, as shown in Figure 14c. The machine modal frequency changes at different positions, as shown in Figure 15a.

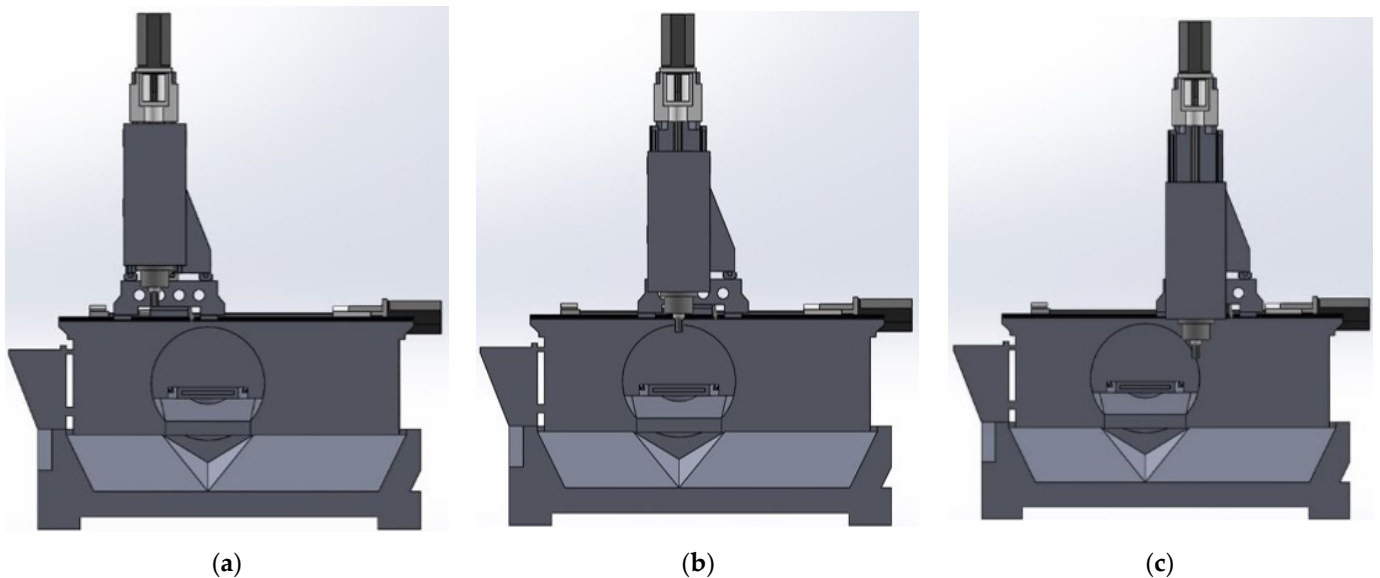
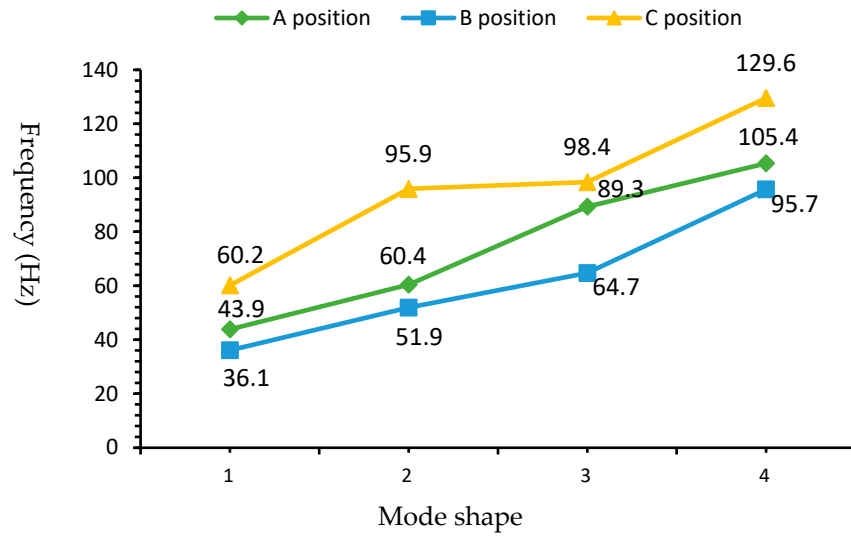
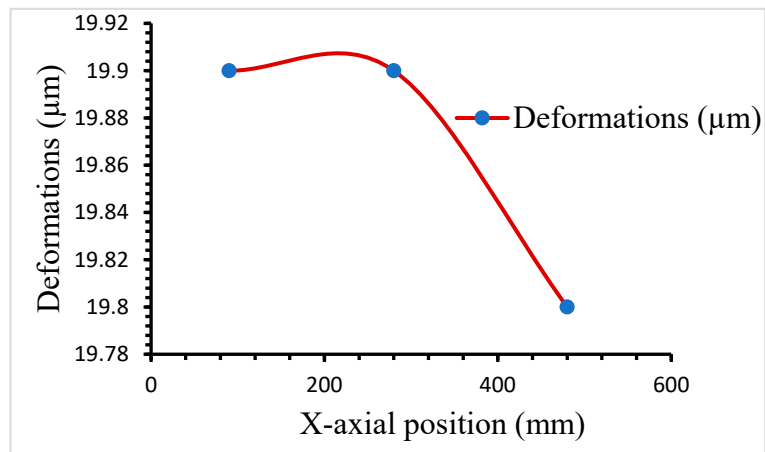


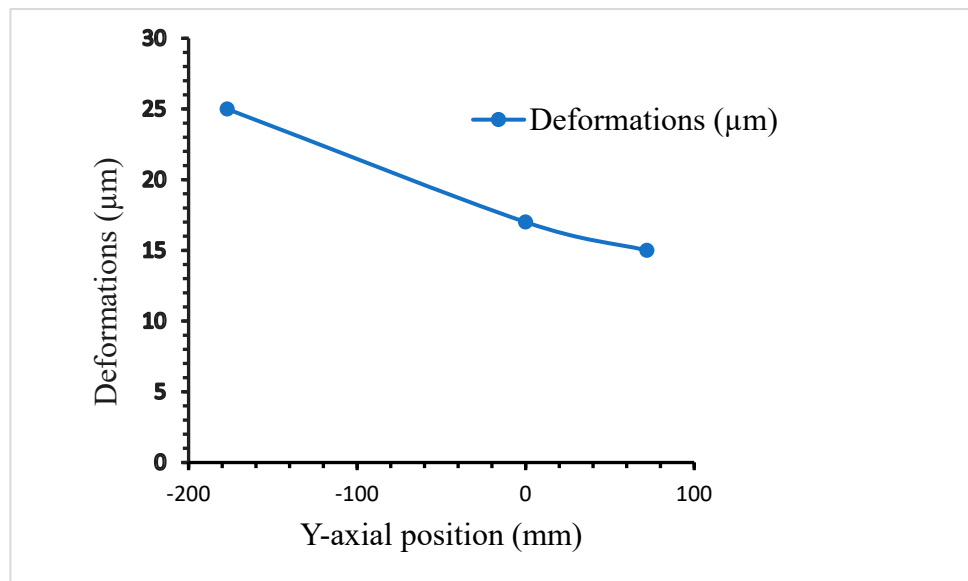
Figure 14. (a–c) shows five-axis machine tool at positions A, B, and C, respectively.



(a)

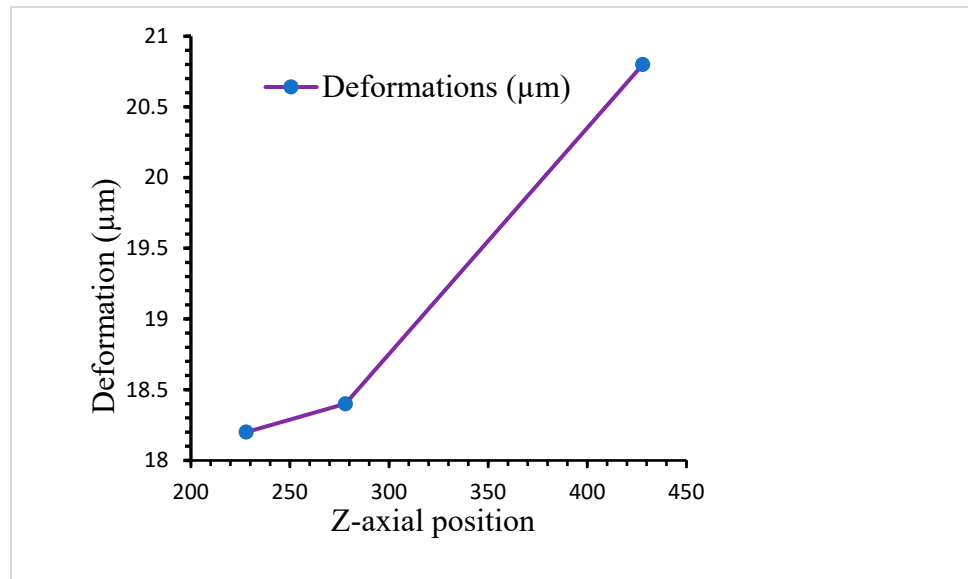


(b)

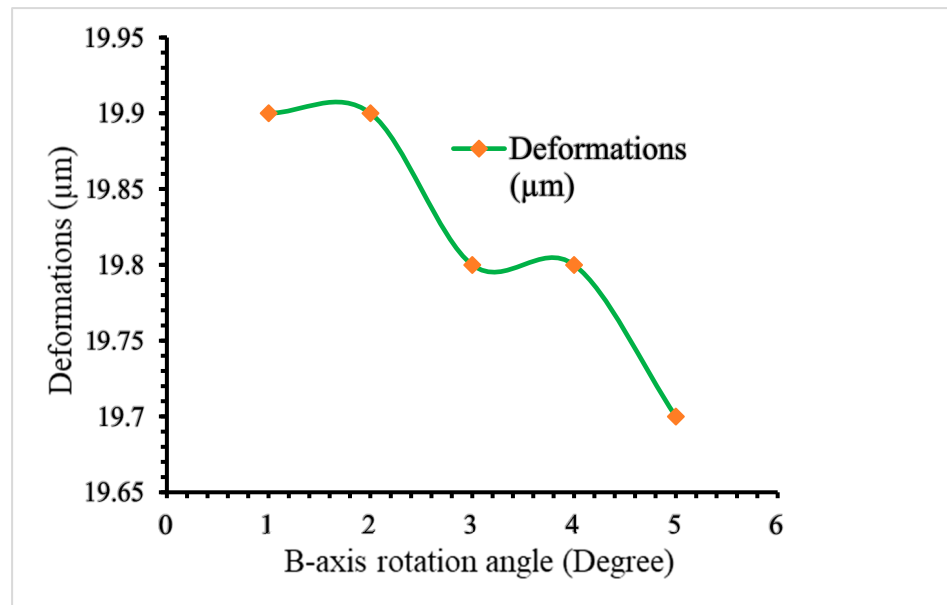


(c)

Figure 15. Cont.



(d)



(e)

Figure 15. (a) Variations in modal frequency of the machine at different positions. (b) X-axis relative change trend graph. (c) Y-axis relative change trend graph. (d) Z-axis relative change trend graph. (e) Relationship between B-axis rotation angle and deformation.

Impact of Dynamic Structure on the Accuracy of the Static Structure

In the X-, Y-, and Z-axis moving distance range, we observe the X, Y, and Z axes separately, as shown in Figure 15b–d. The amount of relative deformation between the tool and the work platform and the deformation changes at different processing points enables us to see that the most significant difference is in the Y-axis. Because the machine has a single-axis oscillating mechanism, the magnitude of the relative deformation of the Y-axis is 8.9 μm.

The quantity of space distortion is essentially constant at all angles since the machine’s center of gravity does not change much when the rotating shaft rotates. As a result, during cutting, the machine’s precision varies continuously. The rotary table is −30, 30, 45, 60, and 90°, and the variability is not substantially different, according to the data. As seen in Figure 15e, the difference is within 1 μm.

2.11. Force Flow Explore

Figure 16 illustrates the force transmission path between the action and response forces inside the structure, which is referred to as the force streamline. When designing structural parts, the shorter the force streamline, the higher the rigidity. When a force of 1000 N is applied in the X-axis direction, the relative deformation amount from the rotating base (C) to the tool base is 26.98 μm , higher than other relative deformation amounts. The relative deformation amount is shown in Table 3. Therefore, if you want to increase the rigidity of the whole machine, you need to adjust the rotating table and improve the structure of the spindle head. The relative maximum deformations (μm) of the machine tool's different components are analyzed in Figure 17.

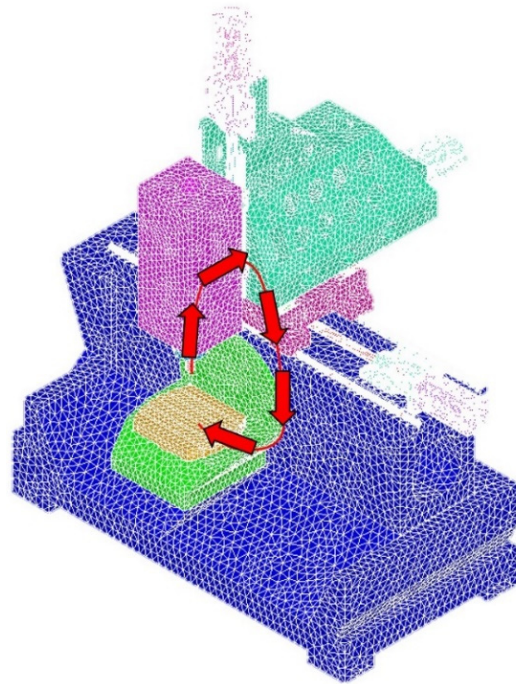


Figure 16. Machine force flow explore.

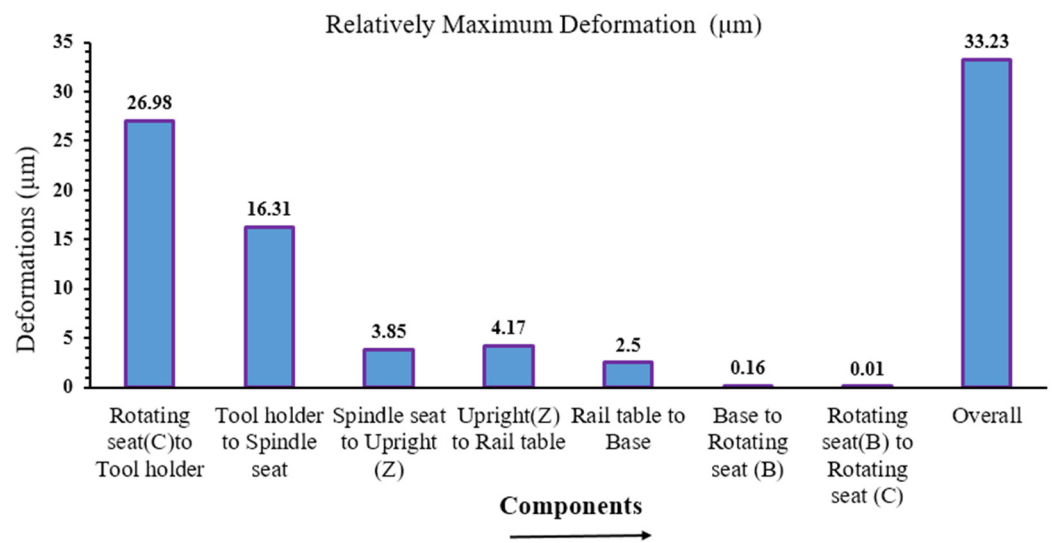


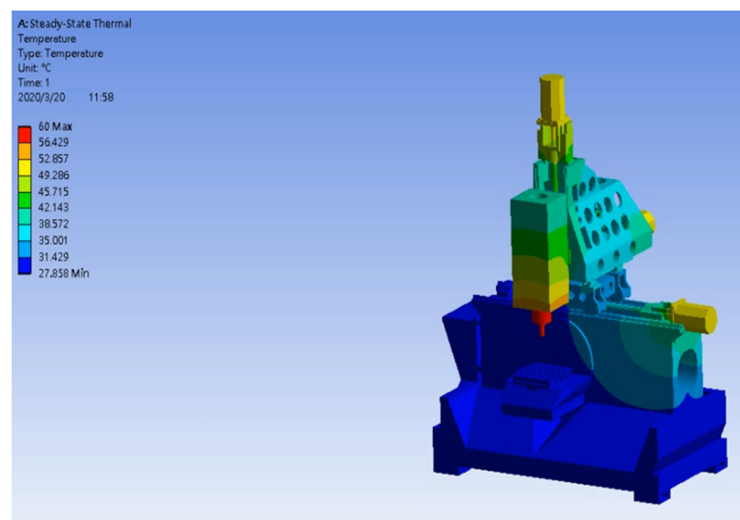
Figure 17. Analysis of relatively maximum deformation (μm).

Table 3. Relative static rigidity analysis results of the complete machine.

Sl. No.	Component Structure	Relatively Maximum Deformation (μm)
1	Rotating seat (C) to Tool holder	26.98
2	Tool holder to Spindle seat	16.31
3	Spindle seat to Upright (Z)	3.85
4	Upright (Z) to Rail table	4.17
5	Rail table to Base	2.5
6	Base to Rotating seat (B)	0.16
7	Rotating seat (B) to Rotating seat (C)	0.01
8	Overall	33.23

2.12. Steady-State Thermal Analysis

The principal aims of conducting a steady-state thermal analysis on a 5-axis vertical milling machine are as follows: ascertaining the temperature distribution throughout crucial components, including the spindle, tool holder, worktable, and drive motors; recognizing possible hot spots that may result in thermal distortion or component degradation; and optimizing the cooling and thermal management systems to guarantee optimal precision and dependable performance. We use the FEM model of the 5-axis machine tool in Ansys 19.2 to perform steady-state thermal analysis. Figure 18 presents the simulation which determines possible hot spots and computes the temperature distribution. The ambient temperature and the film coefficient are two significant elements in this investigation. Considering a film coefficient of $80 \text{ W/m}^2 \text{ }^\circ\text{C}$ and an ambient temperature of $60 \text{ }^\circ\text{C}$, the thermal analysis of the spindle in a 5-axis vertical milling machine offers important insights into its thermal behavior. The spindle's performance and dependability may be improved, guaranteeing accurate and effective machining operations, by comprehending and optimizing these temperature characteristics. This investigation highlights how crucial efficient heat management is for preserving the high-performance milling machines' operational integrity.

**Figure 18.** Simulation of possible hot spots and computation of the temperature distribution.

3. Experimental Modal Testing

Instead of obtaining modal parameters using finite element models (FEMs) like in analytical modal analysis, experimental modal analysis determines modal parameters via physical testing [40]. Vibrational characteristics are obtained via the impact hammer test [19]. Figure 19 shows that the modal experiment used a triaxle acceleration gauge, an

impact hammer, and a spectrum analyzer. The accelerometer’s tapping and measuring spots must first be marked on the model. As seen in Figure 20, the saddle, slide table, column, spindle head, and worktable served as the accelerometer’s primary measuring locations. Each part was cleaned, and the accelerometer was firmly attached at predetermined locations. Accelerometers are available with different degrees of sensitivity; the selection process is based on the structure’s vibration magnitude. The triaxial accelerometer (Endevco MODEL 65-100) utilized in this investigation is described in Table 4. A few places along the specimen received impact hammer impacts. The placements of the sensor are shown by numerical. The impact hammer is specified in Table 5. Every hit was intended to trigger a variety of vibration modes. The data-collecting system recorded the vibrations that resulted from the accelerometers. The Fast Fourier Transform (FFT) was used to process the raw vibration data to transform time-domain signals into frequency-domain data. Figure 21 shows the natural frequencies of the specimen, which were found to be represented by the peaks in the frequency spectrum. Vibration data from many accelerometer locations were analyzed for phase and amplitude, and the mode shapes corresponding to these natural frequencies were retrieved. The test results’ natural frequencies and mode shapes were compared to theoretical forecasts derived from FEA models and earlier experimental findings. The impact hammer test results showed that the specimen’s natural frequencies were 104 Hz, 118 Hz, 125 Hz, and 133 Hz as shown in the Table 6 modal test column.

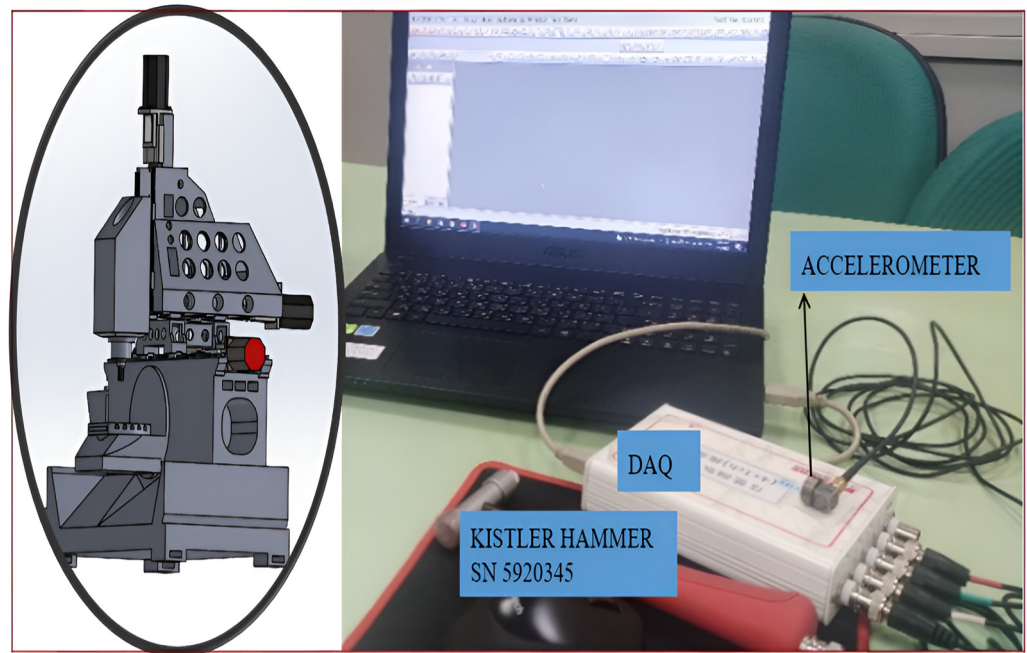


Figure 19. Modal test experiments.

Table 4. Specifications of the accelerometer.

Axis	Sensitivity
X	103.9 mV/g
Y	104.0 mV/g
Z	104.6 mV/g
Dynamic range	±50 g

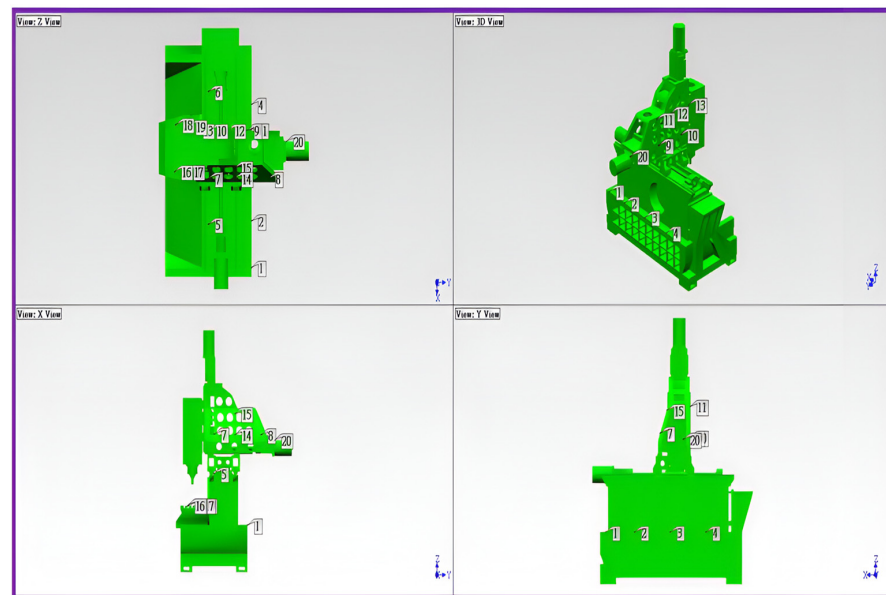


Figure 20. Tapping and measuring spots of the specimen. The positions of the sensors are indicated by numerical values in the figure.

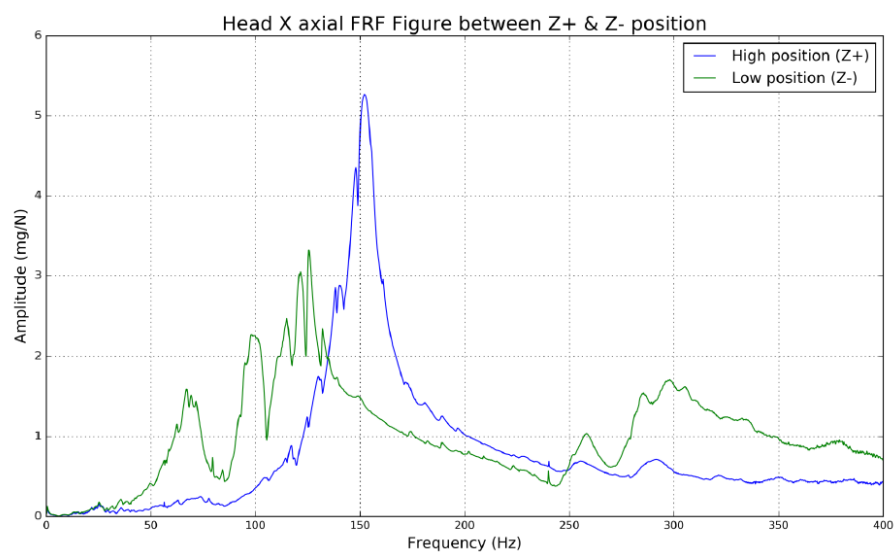
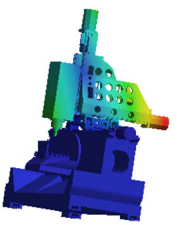
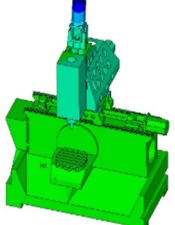
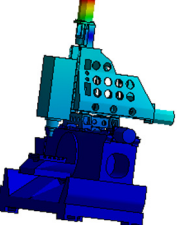
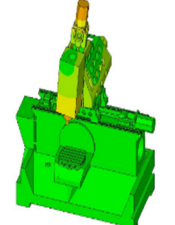
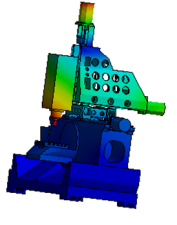
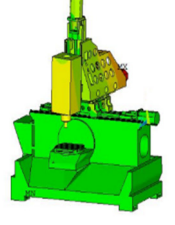
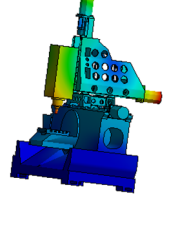
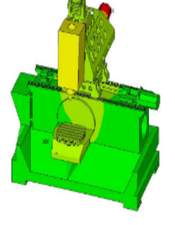


Figure 21. FRF graph obtained from ME'scope.

Table 5. Specifications of impact hammer (KISTLER 9728A200000).

Range of working temperature	−20.671.1 °C
Force range	0–4448 N
Nominal sensitivity	0.2 mv/N
Measuring strength range	0~22.41 N pk
Measuring force peak range	26.689 N pK
Resonance frequency	20 kHz
Rated current	4~20
Impact hammer weight	1.5 Kg
Handle material	Fiberglass with rubber grip
Head diameter	5.1 cm
Overall length	35.6 cm

Table 6. Comparison of modal analysis and experimental modal testing results.

Content	Modal Analysis	Modal Testing	Feature
Mode shape 1			Arbor supports and spindle head vibrations.
Frequency	97.5 Hz	104 Hz	+6.6%
Mode shape 2			Vibrations from the column.
Frequency	110.4 Hz	118 Hz	+6.8%
Mode shape 3			Base section along the Z-axis.
Frequency	115.6 Hz	125 Hz	+8.1%
Mode shape 4			Distortion of the machine saddle along the Z-axis.
Frequency	129.6 Hz	133 Hz	+2.6%

4. Results

Consistency between experimental and analytical results is crucial for engineering verification. When analyzing a model, boundary conditions, material characteristics, outside disturbances, and human activity connected to the signal-measuring apparatus may all result in significant mistakes. Thus, mode shapes between analysis and test results were compared to verify the five-axis machine tool. The measured resonance frequency discrepancies clearly defined the printer structure’s natural resonant frequency and validated the frequency range and theoretical assessments of the structural testing.

4.1. Modal Comparison

The results of the modal test and modal analysis show that the maximum and lowest error ratios are 2.6% and 8.1%, respectively. The pertinent analytical parameters aligned

with the real-world scenario. Table 6 presents the comparison between finite element analysis and test findings.

4.2. Modal Assurance Criteria (MAC) Analysis [41]

The modal assurance criteria (MAC) serve as a gauge for the degree of linearity (or consistency) between modal vector estimations. This offers an extra degree of confidence when assessing a modal vector using various excitation (reference) points or modal parameter estimate techniques. When the MAC value is 1, the two forms are linearly independent, and when it is less than 1, the two shapes are on the same straight line. The majority of computer systems often use color to display magnitude data, such as MAC, in a 2D or 3D graphic, as shown in Figure 22. The details of FEA, EMA, and MAC values are shown in Table 7. We use ME’scope to perform a MAC analysis, and one can better understand the results by seeing the MAC matrix in Figure 23.

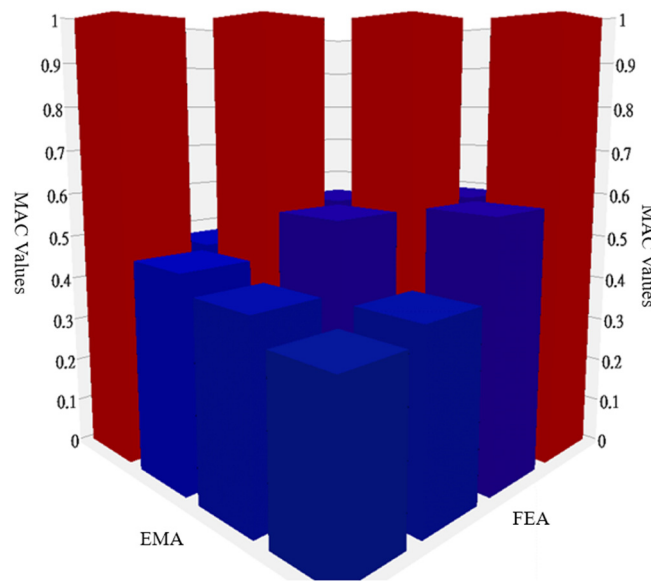


Figure 22. Comparing mode shapes calculated from a finite element simulation using the MAC matrix.

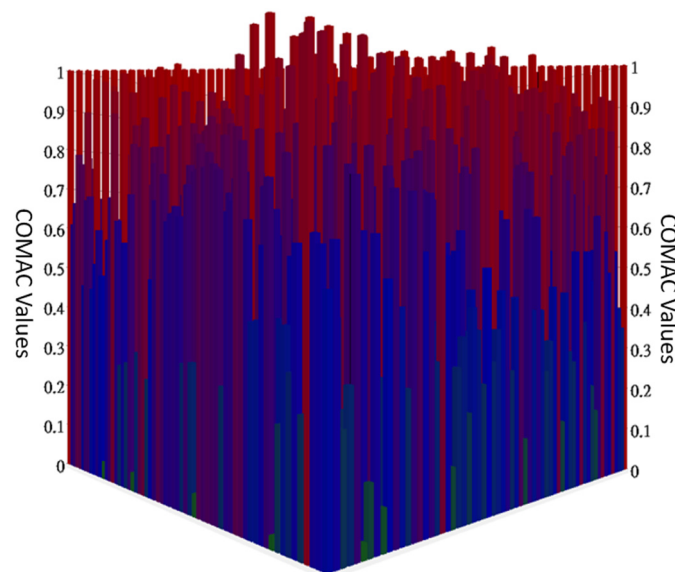


Figure 23. Threshold analysis COMAC matrix.

Table 7. Specifications of EMA, MAC, and FEA values.

Shape Table 1							
Mode Shape	Frequency (or Time) FEA	Frequency (or Time) EMA	MAC Values				
Shape 1	25.3 Hz	22.5 Hz	1	0.636	0.0942	0.0666	
Shape 2	35.3 Hz	31.3 Hz	0.636	1	0.142	0.0444	
Shape 3	45.5 Hz	49.4 Hz	0.0942	0.142	1	0.151	
Shape 4	80.4 Hz	78.1 Hz	0.0666	0.0444	0.151	1	

Modal Assurance Criterion (MAC) Unity

If the modal assurance criterion (MAC) is near unity, it indicates that the modal vectors are consistent but not necessarily correct. Consistency may arise due to the following phenomena:

- Incomplete measurement of modal vectors, with too few response stations included;
- Forced excitation from an unintended source, such as unbalanced rotating equipment;
- Modal vectors consist primarily of coherent noise, potentially reflecting random noise or bias;
- Modal vectors representing the same mode with different arbitrary scaling, differing only by a complex-valued scale factor when normalized.

4.3. Coordinate Modal Assurance Criterion (COMAC)

The Coordinate Modal Assurance Criterion (COMAC) is an expansion of the modal assurance criterion [42]. The COMAC looks for degrees of freedom in measurements that are adversely correlated with low MAC values. A collection of mode pairings, such as analytical versus analytical, experimental against experimental, or experimental versus analytical, are used to compute the COMAC. The set of mode pairs represents all modes of interest in a specific frequency range, but the two modal vectors in each mode pair represent the same modal vector. A value of COMAC will be calculated for each (measurement) degree of freedom for two sets of modes that are to be compared. We use ME’scope to perform the analysis, and one can better understand the results by seeing the COMAC matrix in Figure 23. The threshold analysis COMAC values close to 1 indicate high coherence, while values significantly less than 1 suggest inconsistencies or noise.

5. Conclusions

Currently, with rapid industrial development, the accuracy and efficiency of the five-axis machine structural design configuration requirements and the structural parts design and analysis are extremely important. For overall machining accuracy, this research uses finite element analysis to analyze the entire machine structure, including static and dynamic analyses to improve the machine design method.

- (1) The machine’s weight was 15% less than in the original design model, the material it was exposed to was not strained, and the region of the structure where the force was considerably deformed was reinforced. All of these improvements may effectively increase the stiffness of the machine structure;
- (2) The static analysis was performed when 100 N of force was applied to the blade tip in the X-axis direction. The maximum deformation obtained was 28.7 μm. We also discussed a comparison of the dynamic machine structure trends when it is in different positions. The static stiffness analysis confirms that the designed five-axis machine tool meets the required rigidity standards for precise machining;
- (3) The outcomes of the modal trials were contrasted with the FEA findings. Based on a real modal analysis, the basic FEA parameters and material characteristics were confirmed. The differences in the modal testing findings between the first-order model analysis and the model testing were +6.6%, and for the second, third, and fourth orders the differences were +6.8%, +8.1%, +2.6%, respectively; all of these differences were within acceptable bounds. A high degree of correlation between the mode forms under comparison is indicated by a good MAC result;

- (4) The COMAC analysis provided valuable insights into the consistency and reliability of the modal vectors for the five-axis machine tool design. The high COMAC values across most DOFs confirm the robustness of the modal analysis, while the lower values at certain locations highlight areas for potential improvement. Overall, the COMAC results reinforce the validity of the structural dynamics assessment conducted in this research;
- (5) The optimization of the five-axis machine tool design successfully met the objectives of weight reduction, stiffness enhancement, and cost efficiency. Advanced optimization techniques and finite element analysis provided a robust framework for improving machine tool performance. These findings demonstrate the potential of optimization in advancing engineering design and achieving superior outcomes;
- (6) To comprehend the thermal behavior of a five-axis vertical milling machine, steady-state thermal analysis is essential. This research aids in the optimization of thermal management systems, assuring accurate and dependable operation by detecting temperature distributions and possible hot spots. In order to maximize thermal distortion reduction, achieve high precision in machining processes, and prolong machine life, it is imperative to maintain stable temperature conditions;
- (7) Future work could explore further refinements in enhancing the FE model, material selection, and structural configurations to achieve additional improvements.

Author Contributions: Conceptualization, R.B. and T.-C.C.; methodology, R.B.; software, J.-S.Y.; validation, R.B., T.-C.C. and J.-S.Y.; formal analysis, T.-C.C.; investigation, R.B.; resources, R.B.; data curation, J.-S.Y.; writing—original draft preparation, R.B.; writing—review and editing, R.B.; visualization, J.-S.Y.; supervision, T.-C.C.; project administration, T.-C.C.; funding acquisition, T.-C.C. All authors have read and agreed to the published version of the manuscript.

Funding: The authors would like to sincerely thank the National Science and Technology Council for their invaluable support and contributions to this research and for supporting this study (grant numbers 111-2221-E-150-024-MY2 and 111-2622-E-150-009).

Data Availability Statement: The original contributions presented in the study are included in the article, further inquiries can be directed to the corresponding author.

Conflicts of Interest: The authors declare no conflicts of interest.

References

1. Wang, Y.; Dong, W.; Zhang, S.; Tang, Z.; Wang, L.; Liu, Y. Design and development of a five-axis machine tool with high accuracy, stiffness and efficiency for aero-engine casing manufacturing. *Chin. J. Aeronaut.* **2022**, *35*, 485–496. [[CrossRef](#)]
2. Khan, A.W.; Wuyi, C. Systematic geometric error modeling for workspace volumetric calibration of a 5-axis turbine blade grinding machine. *Chin. J. Aeronaut.* **2010**, *23*, 604–615. [[CrossRef](#)]
3. Yang, B.; Zhang, G.; Ran, Y.; Yu, H. Kinematic modeling and machining precision analysis of multi-axis CNC machine tools based on screw theory. *Mech. Mach. Theory* **2019**, *140*, 538–552. [[CrossRef](#)]
4. Ibaraki, S.; Oyama, C.; Otsubo, H. Construction of an error map of rotary axes on a five-axis machining center by static R-test. *Int. J. Mach. Tools Manuf.* **2011**, *51*, 190–200. [[CrossRef](#)]
5. Liu, K.; Li, T.; Liu, H.; Liu, Y.; Wang, Y. Analysis and prediction for spindle thermal bending deformations of a vertical milling machine. *IEEE Trans. Ind. Inform.* **2019**, *16*, 1549–1558. [[CrossRef](#)]
6. Liu, J.; Ma, C.; Wang, S. Data-driven thermal error compensation of linear x-axis of worm gear machines with error mechanism modeling. *Mech. Mach. Theory* **2020**, *153*, 104009. [[CrossRef](#)]
7. Jin, L.; Yan, Z.; Xie, L.; Gou, W.; Tang, L. An experimental investigation of spindle rotary error on high-speed machining center. *Int. J. Adv. Manuf. Technol.* **2014**, *70*, 327–334. [[CrossRef](#)]
8. Shi, S.; Lin, J.; Wang, X.; Zhao, M. A hybrid three-probe method for measuring the roundness error and the spindle error. *Precis. Eng.* **2016**, *45*, 403–413. [[CrossRef](#)]
9. Wang, J.; Niu, W.; Ma, Y.; Xue, L.; Cun, H.; Nie, Y.; Zhang, D. A CAD/CAE-integrated structural design framework for machine tools. *Int. J. Adv. Manuf. Technol.* **2017**, *91*, 545–568. [[CrossRef](#)]
10. Wang, L.; Wang, D.; Wang, B.; Li, W. Development of an oscillating grinding machine tool based on error analysis. *Sci. China Technol. Sci.* **2020**, *63*, 912–922. [[CrossRef](#)]
11. Chan, T.-C.; Reddy, S.V.V.S.; Ullah, A.; Roy, B. Effect of spatial moving structure and topology optimization of the CNC turning machine tools. *Int. J. Adv. Manuf. Technol.* **2023**, *129*, 2969–2987. [[CrossRef](#)]

12. Shen, L.; Ding, X.; Li, T.; Kong, X.; Dong, X. Structural dynamic design optimization and experimental verification of a machine tool. *Int. J. Adv. Manuf. Technol.* **2019**, *104*, 3773–3786. [[CrossRef](#)]
13. Wu, J.; Yu, G.; Gao, Y.; Wang, L. Mechatronics modeling and vibration analysis of a 2-DOF parallel manipulator in a 5-DOF hybrid machine tool. *Mech. Mach. Theory* **2018**, *121*, 430–445. [[CrossRef](#)]
14. Chan, T.-C.; Chang, C.-C.; Ullah, A.; Lin, H.-H. Study on kinematic structure performance and machining characteristics of 3-axis machining center. *Appl. Sci.* **2023**, *13*, 4742. [[CrossRef](#)]
15. Gegg, B.C.; Suh, S.C.S.; Luo, A.C.J. Modeling and Theory of Intermittent Motions in a Machine Tool With a Friction Boundary. *J. Manuf. Sci. Eng.* **2010**, *132*, 041001. [[CrossRef](#)]
16. Zhou, H.; Hu, P.; Tan, H.; Chen, J.; Liu, G. Modelling and compensation of thermal deformation for machine tool based on the real-time data of the CNC system. *Procedia Manuf.* **2018**, *26*, 1137–1146. [[CrossRef](#)]
17. Soori, M.; Jough, F.K.G.; Dastres, R.; Arezoo, B. A Review in Capabilities and Challenges of 5-Axis CNC Milling Machine Tool Operations. *Preprint* **2024**. [[CrossRef](#)]
18. Chan, T.-C.; Hong, Y.-P.; Wang, Y.-C.; Wu, S.-H. Optimization design of the composite structure of linear motor machine tools. *J. Mech. Eng. Autom.* **2019**, *9*, 219–224. [[CrossRef](#)]
19. Chan, T.-C.; Medarametla, S.V.; Behera, R. Analyzing positional accuracy and structural efficiency in additive manufacturing systems with moving elements. *Results Eng.* **2024**, *23*, 102344. [[CrossRef](#)]
20. Chan, T.-C.; Hong, Y.-P.; Yu, J.-H. Effect of Moving Structure on the Spatial Accuracy and Compensation of the Coordinate Measuring Machine. *Int. J. Precis. Eng. Manuf.* **2021**, *22*, 1551–1561. [[CrossRef](#)]
21. Revanasiddesh, B.; Taj, A.P.; Kumar, N.N.; Suresh, B. Extraction of modal parameters of CNC lathe bed using finite element and experimental method. *Mater. Today Proc.* **2020**, *24*, 398–405. [[CrossRef](#)]
22. Lima, D.Z.; Dezan, D.J.; Gasparin, E.E.; Salviano, L.O.; Yanagihara, J.I.; Ferreira, W.G. Modal analysis and structural optimization of integrated bladed disks and centrifugal compressor impellers. *Struct. Multidiscip. Optim.* **2024**, *67*, 40. [[CrossRef](#)]
23. Ramesha, C.; Abhijith, K.; Singh, A.; Raj, A.; Naik, C.S. Modal analysis and harmonic response analysis of a crankshaft. *Int. J. Emerg. Technol. Adv. Eng.* **2015**, *5*, 323–327. [[CrossRef](#)]
24. Ghani, M.U.; Abukhshim, N.A.; Sheikh, M. An investigation of heat partition and tool wear in hard turning of H13 tool steel with CBN cutting tools. *Int. J. Adv. Manuf. Technol.* **2008**, *39*, 874–888. [[CrossRef](#)]
25. Suresh, R.; Basavarajappa, S.; Samuel, G. Predictive modeling of cutting forces and tool wear in hard turning using response surface methodology. *Procedia Eng.* **2012**, *38*, 73–81. [[CrossRef](#)]
26. Ulrika, L.; Henrik, W.; Artem, K. A methodology for strain-based fatigue damage prediction by combining finite element modelling with vibration measurements. *Eng. Fail. Anal.* **2021**, *121*, 105130. [[CrossRef](#)]
27. Chan, T.-C.; Yang, J.-S. Optimized Design and Performance Study of High Speed Five-Axis Machine Tools. In Proceedings of the ASME 2020 International Design Engineering Technical Conferences and Computers and Information in Engineering Conference, Virtual, 17–19 August 2020.
28. Kim, S.; Kim, S.; Kim, T.; Choi, S.; Lee, T.H.; Park, J.S.; Jung, S.-H. Topology optimization of reactive material structures for penetrative projectiles. *Def. Technol.* **2022**, *18*, 1205–1218. [[CrossRef](#)]
29. De Lacalle, L.L.; Lamikiz, A.; Salgado, M.; Herranz, S.; Rivero, A. Process planning for reliable high-speed machining of moulds. *Int. J. Prod. Res.* **2002**, *40*, 2789–2809. [[CrossRef](#)]
30. Calleja, A.; Bo, P.; González, H.; Bartoň, M.; López de Lacalle, L.N. Highly accurate 5-axis flank CNC machining with conical tools. *Int. J. Adv. Manuf. Technol.* **2018**, *97*, 1605–1615. [[CrossRef](#)]
31. González, H.; Calleja, A.; Pereira, O.; Ortega, N.; López de Lacalle, L.N.; Barton, M. Super Abrasive Machining of Integral Rotary Components Using Grinding Flank Tools. *Metals* **2018**, *8*, 24. [[CrossRef](#)]
32. Bo, P.; González, H.; Calleja, A.; de Lacalle, L.N.L.; Bartoň, M. 5-axis double-flank CNC machining of spiral bevel gears via custom-shaped milling tools—Part I: Modeling and simulation. *Precis. Eng.* **2020**, *62*, 204–212. [[CrossRef](#)]
33. Artetxe, E.; González, H.; Calleja, A.; Valdivielso, A.F.; Polvorosa, R.; Lamikiz, A.; Lacalle, L.N.L.D. Optimised methodology for aircraft engine IBRs five-axis machining process. *Int. J. Mechatron. Manuf. Syst.* **2016**, *9*, 385–401. [[CrossRef](#)]
34. Möhring, H.-C.; Wiederkehr, P.; Erkorkmaz, K.; Kakinuma, Y. Self-optimizing machining systems. *CIRP Ann.* **2020**, *69*, 740–763. [[CrossRef](#)]
35. Pálmai, Z.; Kundrák, J.; Felhő, C.; Makkai, T. Investigation of the transient change of the cutting force during the milling of C45 and X5CrNi18-10 steel taking into account the dynamics of the electro-mechanical measuring system. *Int. J. Adv. Manuf. Technol.* **2024**, *133*, 163–182. [[CrossRef](#)]
36. Yu, Y.; Zhang, S.; Li, H.; Wang, X.; Tang, Y. Modal and Harmonic Response Analysis of Key Components of Ditch Device Based on ANSYS. *Procedia Eng.* **2017**, *174*, 956–964. [[CrossRef](#)]
37. Zaghbani, I.; Songmene, V. Estimation of machine-tool dynamic parameters during machining operation through operational modal analysis. *Int. J. Mach. Tools Manuf.* **2009**, *49*, 947–957. [[CrossRef](#)]
38. Wu, Z.; Xu, C.; Zhang, J.; Yu, D.; Feng, P. Modal and harmonic response analysis and evaluation of machine tools. In Proceedings of the 2010 International Conference on Digital Manufacturing & Automation, Changcha, China, 18–20 December 2010; pp. 929–933.
39. Chan, T.-C.; Wu, S.-C.; Ullah, A.; Farooq, U.; Wang, I.H.; Chang, S.-L. Integrating numerical techniques and predictive diagnosis for precision enhancement in roller cam rotary table. *Int. J. Adv. Manuf. Technol.* **2024**, *132*, 3427–3445. [[CrossRef](#)]

40. Carré, M.; Haake, S. An examination of the Clegg impact hammer test with regard to the playing performance of synthetic sports surfaces. *Sports Eng.* **2004**, *7*, 121–129. [[CrossRef](#)]
41. Allemang, R.J. The modal assurance criterion—twenty years of use and abuse. *Sound Vib.* **2003**, *37*, 14–23.
42. Fuentes, H.P.; Zehn, M. Application of the Craig-Bampton model order reduction method to a composite structure: MACco, COMAC, COMAC-S and eCOMAC. *Open Eng.* **2016**, *6*, 185–198. [[CrossRef](#)]

Disclaimer/Publisher’s Note: The statements, opinions and data contained in all publications are solely those of the individual author(s) and contributor(s) and not of MDPI and/or the editor(s). MDPI and/or the editor(s) disclaim responsibility for any injury to people or property resulting from any ideas, methods, instructions or products referred to in the content.